Article

Projected Rainfall Triggered Landslide Susceptibility Changes in the Hengduan Mountain Region, Southwest China under 1.5–4.0 °C Warming Scenarios Based on CMIP6 Models

Huaxiang Yin [1,†], Jiahui Zhang [2,†], Sanjit Kumar Mondal [3], Bingwei Wang [1], Lingfeng Zhou [4], Leibin Wang [5] and Qigen Lin [1,*]

1   Institute for Disaster Risk Management/School of Geographical Sciences, Nanjing University of Information Science & Technology, Nanjing 210044, China
2   Academy of Disaster Reduction and Emergency Management, Ministry of Emergency Management and Ministry of Education, Beijing Normal University, Beijing 100875, China
3   Department of Atmospheric Sciences/Irreversible Climate Change Research Center, Yonsei University, Seoul 03722, Republic of Korea
4   State Key Laboratory of Environmental Criteria and Risk Assessment, Chinese Research Academy of Environmental Sciences, Beijing 100012, China
5   School of Geographical Sciences, Hebei Normal University, Shijiazhuang 050024, China
*   Correspondence: linqigen@mail.bnu.edu.cn
†   These authors contributed equally to this work.

Abstract: Landslides are one of the most prevalent environmental disasters in the Hengduan Mountain Region. Landslides lead to severe economic damage and property loss, as well as fatalities. Furthermore, they tend to increase in the context of climate change. The purpose of this study is to comprehensively assess landslide susceptibility across the Hengduan Mountain Region in southwest China. Specifically, the analysis is focused on the eastern boundary of the Tibetan Plateau within the context of future climate change scenarios, which are based on the latest Coupled Model Intercomparison Project Phase 6 (CMIP6) global climate model ensemble. The Generalized Additive Model (GAM), Random Forest (RF), and Light Gradient Boosting Machine (LightGBM) were selected in order to map landslide susceptibility within the context of 1.5–4.0 °C warming scenarios. This was achieved by considering the changes in extreme rainfall that exceeded the landslide triggering thresholds. The results show that the frequency over extreme rainfall thresholds (FOERT) tend to increase in conjunction with warming targets, thereby ranging from 2.3/a (at a 1.5 °C warming) to 9.0/a (at a 4.0 °C warming) on average. Such elevated extreme precipitation events contribute to an increase in projected future zones of high landslide susceptibility when compared to the historical baseline period ranging from −1.2% (at a 1.5 °C warming) to 4.0% (at a 4.0 °C warming) using different machine learning models. Moreover, the extent of high susceptibility zones increases more significantly in the context of 4.0 °C warming when compared to the historical baseline results. These results indicate the importance of limiting the global temperature rise to 1.5 as well as 2 °C. The high landslide susceptibility zones estimated by the CMIP6 multi-models ensemble are mainly located in the central and southeastern regions of the Hengduan Mountain Region. The possible changes in terms of introducing extreme precipitation in order to assess landslide susceptibility in the context of climate change that is proposed in this study may be further applied to additional study areas. These projections under different targets can provide scientific guidelines for the purposes of the development of climate change adaptation strategies.

Keywords: landslide susceptibility; machine learning; climate change; extreme rainfall; CMIP6; Hengduan Mountain Region

1. Introduction

Climate change and global warming are the most dramatic environmental issues of the 21st century [1]. According to the Intergovernmental Panel on Climate Change (IPCC) Special Report on Global Warming of 1.5 °C, rising temperatures are closely related to the frequency of extreme weather, while the accompanying natural disasters can greatly threaten human lives [2]. A growing number of studies in recent years have shown that landslides are projected to become more frequent in the context of global climate warming [3–5]. However, assessing future landslide susceptibility is challenging, which is a result of the complex transition process from climate change to landslide impacts. As the impact of climate change in respect of landslides varies dramatically across geographic regions, time periods, and socio-economic development scenarios, such impacts may be long-term or short-term and can also manifest in a direct or indirect manner [6–8].

There is a close correlation between landslides in mountainous areas and climatic processes, such as extreme rainfall [9]. Notably, heavy rainfall is understood to be a key trigger of shallow landslides. Most of the current studies utilize static rainfall indicators, such as average annual rainfall, but do not consider the variation of extreme rainfall under future climate change scenarios [10]. Certain scholars use global climate models (GCMs) in order to derive future climate variables. The process would be to feed the GCMs data output to statistical or physical process models in order to model possible changes in future landslides [11–14]. However, the assessment of future landslide hazards while using GCMs data presents complex characteristics that require further investigation [13]. The results based on the CMIP5 GCMs showed that future landslides are expected to increase in the Markazi province of Iran due to the influence of climate change and land-use impacts [11]. In contrast, the opposite result showed a decreasing trend in areas of high landslide susceptibility in the Peloritani Mountains, Italy, even with the potential impact of future climate change [14]. Therefore, the frequency of landslides under the influence of climatic conditions is uncertain and requires corroboration by further relevant studies.

In addition, a review based on 139 studies related to the impact of climate change on landslides from 1983–2018 indicates that most of the current study areas are in certain European countries, such as the United Kingdom and Italy [8]. In comparison, the impact of landslides cannot be ignored in some parts of Asia, due to the continent's high population exposure. A few studies have shown that landslides tend to increase in southwestern China, when taking into account climate change effects [15–17]. However, a study in a large area cannot be ignored due to the bias caused by spatial and temporal heterogeneity. Therefore, this study selects the areas of interest within the Hengduan Mountain Region in Southwest China, where landslides are prone to occur due to their complex and diverse geological features, as well as due to the presence of frequent extreme rainfall [18]. Indeed, studies have also shown that the high frequency of landslides in the region—that is, the frequent occurrence of flow-type landslides, frequent seismic activities, frequent heavy rainfall events, and intensified human activities have resulted in serious damage [19,20]. The complex topographic features and climatic conditions render the region highly susceptible to large-scale geological hazards. Predicting the probability of future landslide hazards can provide corresponding scientific support to instruct the development of landslide risk mitigation strategies. It must be noted that most of the current studies have used the output of CMIP5. With the accessible of the Coupled Model Intercomparison Project Phase 6 (CMIP6) output, several studies have shown that CMIP6 rainfall simulations improved when compared to the previous iterations [21,22]. The CMIP6 multi-model ensemble can more reasonably reproduce the mean values of climate variables and the spatial distribution of precipitation; in addition, it generally exhibits a higher level of skill in simulating extreme precipitation indices over China [23,24].

In this study, the aim is to use CMIP6 global climate model data combined with the landslide susceptibility models in order to explore the future landslide conditions in the Hengduan Mountains on the eastern boundary of the Tibetan Plateau in southwestern China—specifically in respect of the change in extreme rainfall in the context of different

warming scenarios. The objectives of this study are to: (a) project future changes in extreme precipitation in the Hengduan Mountains; (b) use landslide susceptibility models to determine how landslide susceptibility will change in the future as a result of extreme rainfall variations; and (c) to compare the differences in the projected results obtained by different machine learning models.

2. Study Area and Materials

2.1. Research Area and Historical Landslide Database

The Hengduan Mountain Region covers an area of 600,000 square kilometers and is situated within the Yunnan–Guizhou Plateau, the Qinghai–Xizang Plateau, and the border between Sichuan and Tibet (Figure 1). The topography of the study area is in an elevated position in the northwest and in a lowered position in the southeast. The area possesses high mountains and canyons, as well as a great relative height discrepancy. The altitude ranges from 90 to 7121 m, with many peaks exceeding 6000 m [25]. With an average gradient is 23.7°, and a maximum gradient is 78.4°, the terrain is steep and undulating. Due to its unique topographic conditions, landslides are prone to occur.
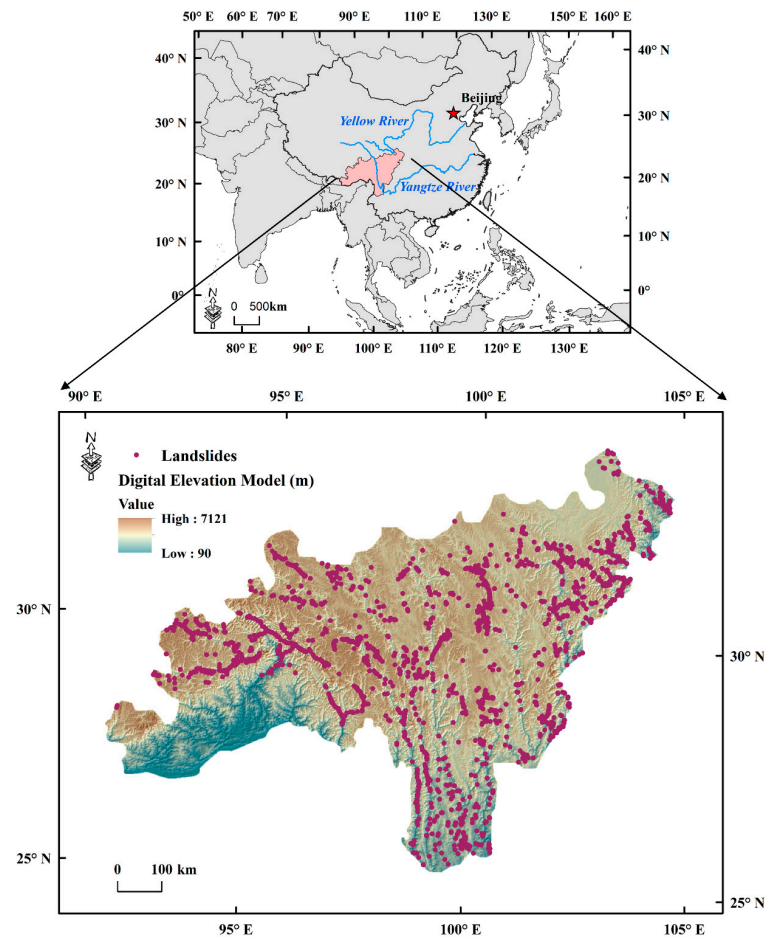

Figure 1. Study area and historical landslide data.

The territory spans the subtropical, highland, and boreal areas and is influenced by the southwest monsoon in the west, thus resulting in moist and mild topographic rainfall; moreover, the leeward valleys are arid [26]. The rivers possess rapid currents and abrupt drop-offs. Precipitation varies greatly between wet and dry seasons (i.e., May to September and October to April), with wet seasons receiving 70% of the total precipitation.

The area is tectonically active; furthermore, the lithology spans the Lower Paleozoic to the Triassic, with marine sediments, such as clastic and carbonate—as well as gneisses,

marble, sandstone, and shale—which are all scattered throughout the valley [27]. The abundant geological, environmental conditions for the development of geological hazards are provided by intense geotectonic activity, active neotectonic movement, as well as complex and diverse stratigraphic lithology. The study area combines geomorphological features and climatic conditions that are prone to geological hazards, which is imperative to explore the potential impact of rainfall conditions that induce geological hazards.

The creation of a historical landslide database is a key procedure in developing landslide susceptibility model [28]. The China Geological Survey has gradually carried out detailed investigations of six geological hazards, including ground fissures, avalanches, landslides, ground subsidence, ground collapse, and mudslides, since 2005. Among these, landslides of the movement type are the most dangerous and destructive. The historical landslide database used in this work derives from this survey, which maps each landslide as a point and includes 2223 rainfall-induced landslides of flow type mass-movement that were recorded in the Hengduan Mountain Region [29]. Furthermore, we use vector points in GIS software in order to describe the central area where landslides occur.

2.2. Landslide Conditioning Factors

Environmental factors affecting landslides can be classified as: climatic; geological and soil; topographic; land cover; vegetation cover; hydrological; and human activity factors [30]. The rise in landslide frequency due to land use change is assumed to be a key factor in respect of the increase in landslide hazards [31,32]. The soil moisture index possesses a significant effect in respect of landslides [33]; in addition, soil typology influences the incidence of erosion, drainage, as well as the impacts that occur in relation to landslides [34]. DEM information directly represents elevation information within a region and can be used as a basis for elevation change, especially in areas with large drop-offs. The slope is the most commonly utilized predictor in data-driven landslide susceptibility modeling and is often served as the fundamental static independent variable for landslide occurrence. As a measure of topographic change, the curvature is influenced by elevation change [35]. Lithology, in addition to topographic properties, is a major factor in landslide occurrence due to the fact that it straightforwardly influences the intensity and permeability of the geotechnical soil. It is an important determinant in the context of landslide susceptibility modeling [36]. Furthermore, the nature of the soil and thus the area of the watershed may be influenced by the hydrology and runoff in a given area [37]. Meanwhile, the vegetation cover may influence the distribution of landslide occurrence. The normalized difference vegetation index (NDVI) was chosen in order to represent the forest cover that affect the happenings of landslides in the mountain area [38].

In current work, we utilized a uniform raster resolution of 1 km. We chose six categories of landslide conditioning factors (LCFs), which are: topographic factors (i.e., slope, curvature, slope orientation, elevation); geological and soil factors (lithology, soil type); climatic and meteorological environmental factors (multi-year average rainfall, over landslide rainfall threshold); hydrology (curve numbers, soil moisture, drainage density); land use (land use type); and vegetation cover (NDVI). These factors were assessed following the review of the literature for the purposes of analyzing landslides; in addition, such an assessment was also limited by the availability of relevant data. Among these, the elevation data were obtained from the SRTM 90 m spatial resolution data, and the slope (Figure 2a) were derived from the DEM. The hydrological factor curve numbers (CN, Figure 2b) were obtained from Zhao et al. [39]. It must be noted that CN is a dimensionless parameter used to represent a hydrologic index in order to describe the approximation of direct runoff from rainfall events in a specific area. It is related to soil moisture, soil type, slope, and other influencing factors. It is widely used in the field of landslide susceptibility research [40]. Among the geological and soil factors, the soil type (Figure 2g) were obtained from the Resource and Environmental Science and Data Center, Chinese Academy of Sciences (RESDC). A total of 10 soil types were leached soil (10); semi-leached soil (11); arid soil (13); incipient soil (15); semi-hydrogenated soil (16); hydrogenated soil (17); anthropogenic soil (19); alpine

soil (20); ferroaluminous soil (21); and rock (23). The soil moisture (Figure 2d) is from the Global High-Resolution Soil–Water Balance dataset, which provides hydrological raster data describing actual evapotranspiration and soil water deficits with a resolution of 30 arc seconds [41]. The soil moisture data detailed in this study are the annual average soil water content as a percentage of the maximum soil water content during the evaporation period. The lithology map (Figure 2e) was acquired from the Global Lithology Map database with 11 lithological classifications, including Mixed Sedimentary Rocks (SM); Carbonate Sedimentary Rocks (SC); Siliciclastic Sedimentary Rocks (SS); Metamorphics Rocks (MT); Acid Plutonic Rocks (PA); Evaporites (EV); Basic Plutonic Rocks (PB); Intermediate Plutonic Rocks (PI); Intermediate Volcanic Rocks (VI); Unconsolidated Sediments (SU); and Acid Volcanic Rocks (VA). The climate and meteorological factors were obtained from the CN05.1 grid observation dataset and the original spatial resolution of CN05.1 was $0.25° \times 0.25°$ [42]. However, due to the fact that the spatial distribution of precipitation is affected by topographic variations—in order to reduce the influence of topographic spatial heterogeneity on precipitation simulations—the ANUSPLIN climate data interpolation software was used to further interpolate the CN05.1 data, as well as the global climate model data to a 1 km spatial resolution. At the same time, the quantile mapping method was used to process the bias correction of each climate model data in order to reduce the model simulation error. The spatial variability of precipitation is represented by nine climatic indicators, including mean annual rainfall, annual maximum daily rainfall, yearly mean daily maximum rainfall, yearly mean rainfall over 10 mm (days), yearly mean rainfall over 25 mm (days), yearly mean rainfall over 50 mm (days), yearly mean rainfall over a 95% quantile (days), 95% quantile daily precipitation, and frequency over empirical rainfall thresholds. The research thus far only provides the mean annual rainfall (Figure 2c) and the frequency over empirical rainfall thresholds (FOERT, Figure 2h)—which are more relevant to the landslide distribution, due to the approximate spatial pattern of these precipitation variables. The rainfall thresholds of induced landslides for different geomorphic subdivisions in China were constructed by Wang et al., (2021) as a power–law relationship between cumulative event rainfall and rainfall duration based on the historical hydrogeomorphic hazard data set in China (which contains all hydrogeomorphic processes between the defined ranges of flash floods and debris flows) for different geomorphic subdivisions [43]. For the purposes of this study, it is the rainfall threshold curve for the southwest mountainous region that is utilized. The rainfall event time series for each grid point were compared with the threshold values for the southwestern mountainous region. Furthermore, the frequency in respect of exceeding the rainfall threshold curve was counted and finally presented in the form of a grid. The land use (Figure 2f) map of the year 2005 was obtained from the RESDC in five groups, which are: Meadowland (Me); Arable land (Ar); Settlements and Artificial land (SA); Forest land (Fo); and Unutilized land (Un). The annual mean NDVI of vegetation cover (Figure 2i) was also acquired from the RESDC. The drainage density (Figure 2j) data were acquired from the HydroSHEDS database [44].
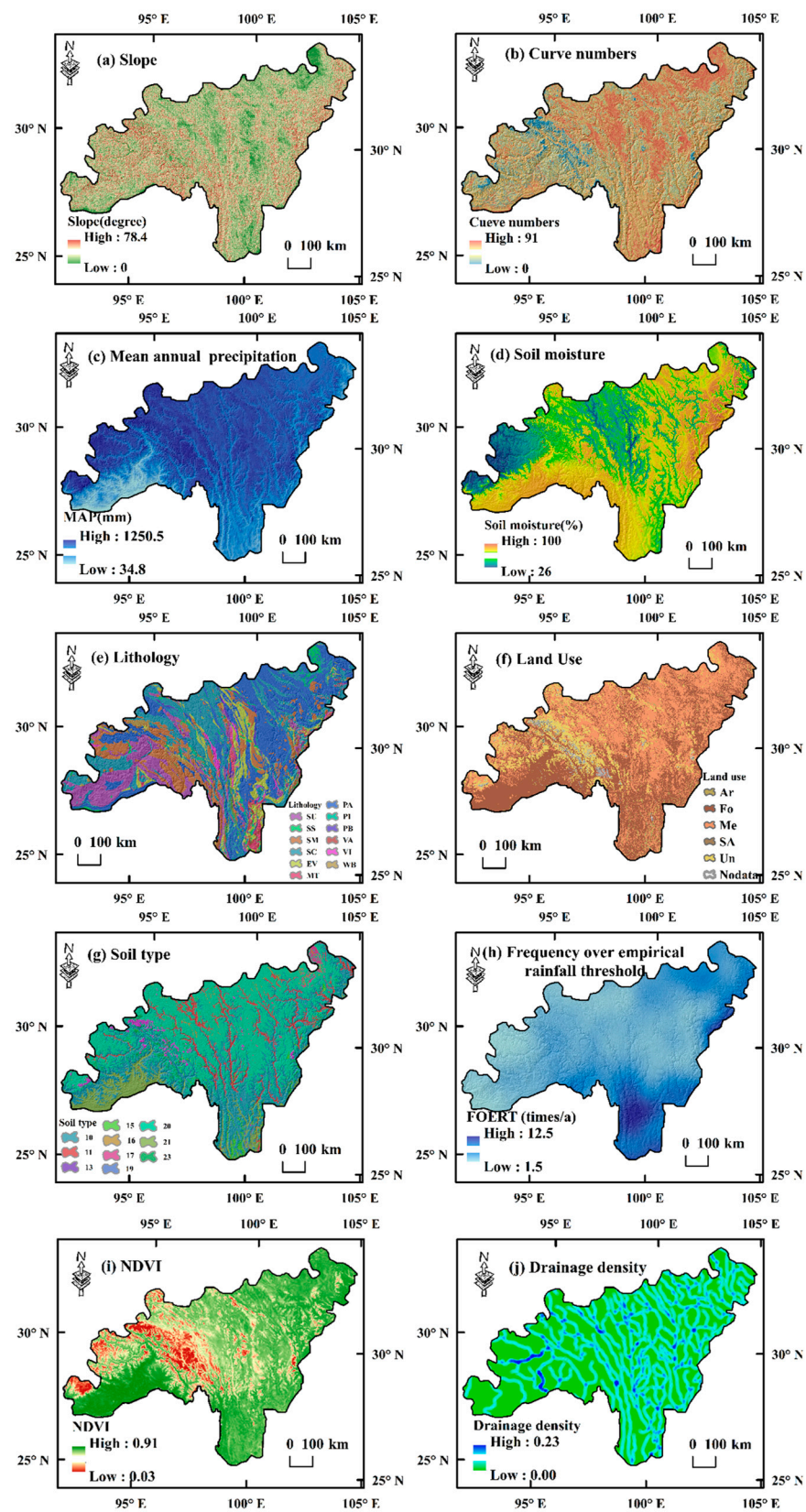
Figure 2. Landslide conditional factors: (**a**) slope; (**b**) curve numbers; (**c**) mean annual rainfall (MAP); (**d**) soil moisture; (**e**) lithology; (**f**) land use; (**g**) soil type; (**h**) frequency over empirical rainfall threshold (FOERT); (**i**) mean NDVI; and (**j**) drainage density.

3. Methodology

Figure 3 depicts the flowchart for the modeling process, which is divided into three stages: preparation, landslide susceptibility modeling under consideration of climatic rainfall conditions, and result analysis. During the preparation stage, a total of 2223 historical landslide data for the research region were compiled. This was achieved with the landslide present value set to 1 and a similar amount in respect of the randomly generated non-landslide value set to 0. A landslide susceptibility assessment is a binary classification problem. As such, in order to train the model better, the same number of landslide and non-landslide samples should be used to constitute the dependent variable together [45]. Subsequently, the dataset was stochastically classified into two groups, whereby 70% of the samples were utilized for modeling and the rest were used in respect of the dataset for validation. Data regarding the landslide conditioning factors were preprocessed by checking for multicollinearity and normalization, then determining the dominant influencing factors using the relative importance index.
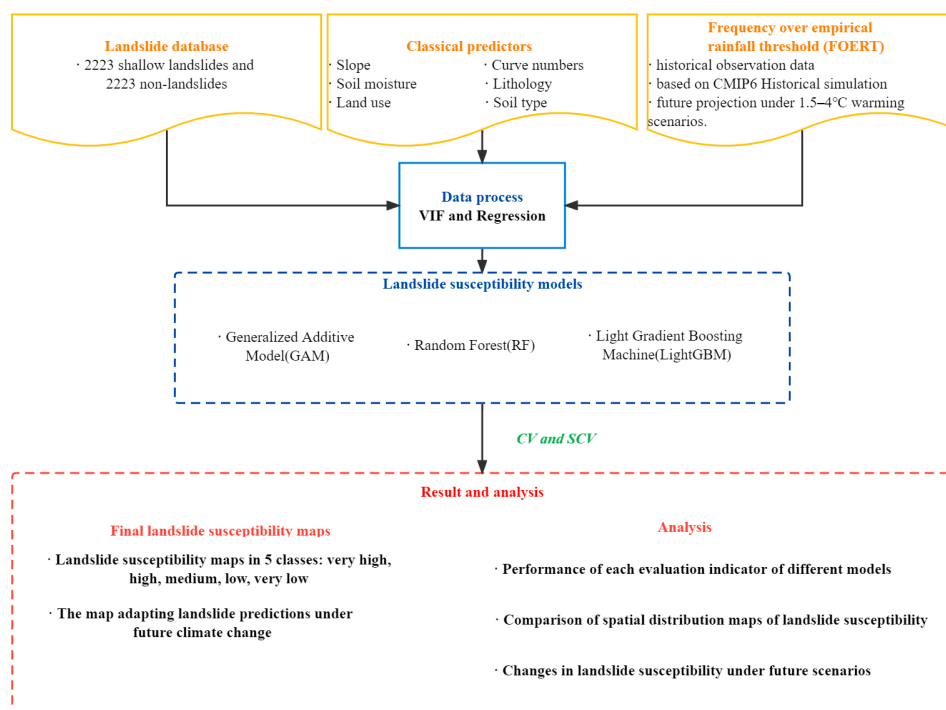

Figure 3. Methodological flowchart of the study.

In the Hengduan Mountain Region, historical rainfall during the period of 1995–2014 are used as the baseline model. After this, the future-projected climate rainfall data were introduced, while landslide susceptibility modeling was performed via using the GAM, RF, and LightGBM. The potential impacts of rainfall in respect of the different warming scenarios were evaluated by comparing the historical and future modeling results, whereby spatial cross-validation was used in order to verify model uncertainty. During the analysis of the results, indicators such as AUC, ACC, and the F1-score were used. In addition, the proportions of different susceptibility levels in respect of the landslide inventory data were calculated. Finally, the correlation between climatic conditions and landslides in the Hengduan Mountain Region was determined. The landslide susceptibility maps under different warming scenarios were obtained. The following sections will present these methods in greater detail.

3.1. Selection of the Dominant Influencing Factors

The choice of independent variables is a crucial procedure in respect of landslide susceptibility models. Moreover, many of the predictor variables considered are believed to be interrelated. Therefore, it is critical to assess these possible predictor variables before deciding which ones to include in the models [46–48]. First, we created kernel density maps of the fishing nets with a spatial resolution of 1 km based on historical landslide samples. Next, we calculated the mean kernel density of the fishing nets and the mean of continuous variables as inputs in respect of the regression analysis, respectively [40]. In this study, all variables were assessed for multicollinearity by applying the variance inflation factor (VIF) and stepwise regression [49]. Then, dominant variables were chosen based on their relative importance. A VIF greater than 5 indicates the possibility of multicollinearity between variables [50]. As such, the formula for calculating VIF is as follows:

$$VIF = \frac{1}{1 - R_i^2} \qquad (1)$$

where R_i represents the negative correlation coefficient of the independent variable and is used in the regression analysis of the independent variable [51]. Relative importance indices—via the consideration of the relative contribution of variables to the total predictable variance—are widely used in the screening of variables [52,53], without making any assumptions regarding the statistical significance associated with a specific predictor variable.

Before modeling, the landslide conditioning factors were normalized in order to remove the scale differences caused by the different units [54]. The normalizing process was carried out using the following equation:

$$Z_{LCF} = \left(\frac{LCF_i - LCF_{\min}}{LCF_{\max} - LCF_{\min}} \right) \qquad (2)$$

where Z_{LCF} is the value after normalization of LCF, LCF_i is the initial value, and $LCF_{\min}$ and $LCF_{\max}$ are the minimum and maximum values of LCF, respectively.

In terms of the likelihood of determining landslide susceptibility, different LCFs contribute differently to various prediction models. As a result, determining the relative value of each LCF can aid in resolving the favorable conditions for landslide occurrences. In order to investigate the relations between LCFs and landslide events, the response of different LCFs in respect of the model is determined by the magnitude of the cross-validation AUROC change after replacing LCFs. Moreover, the ranking of the magnitude of the AUROC change determines the final relative importance ranking of different variables. In other words, the AUROC values of the model, after removing different variables, are obtained and experimented upon several times in the cross-validation process. The ranking is used and understood as the importance of the variables that are afterward derived from the model. This method has been validated several times in respect of assessing the relative importance of the variables that are derived from the model [55,56].

3.2. Landslide Susceptibility Modeling

We chose the GAM, RF, and LightGBM as the base models in this study. These base models have been used to assess the impact of climate change on landslides [57]. The generalized additive model (GAM) is broadly utilized in environmental science for the purposes of modeling landslide susceptibility due to its simplicity and interpretability. More information regarding using the GAM and mixed-effect models in order to estimate landslide susceptibility can be demonstrated in the study of Steger et al., (2021) [58]. Moreover, Pham et al., (2021) utilized a random forest model to in order assess the potential impact of future climatic rainfall regarding landslide modeling in the Markazi Province, Iran. The results showed that random forest model were able to obtain more accurate estimates [11]. The LightGBM (Light Gradient Boosting Machine) implements the framework of the GBDT

algorithm by optimizing the histogram-based decision tree algorithm and one-sided gradient sampling on the traditional eXtreme Gradient Boosting (XGBoost) algorithm—which, in turn, can support efficient parallel training with faster training reactions, less memory occupation, and higher accuracy [59]. It is a novel landslide susceptibility framework that has performed well in various studies [57].

3.3. GCMs for the Projection of Future Extreme Rainfall

Historical simulations and future projections of global climate models were derived from 24 global climate models in respect of the Coupled Model Intercomparison Project Phase 6 (CMIP6). The CMIP6 involves a larger number of global climate models with improved model resolution and physical parameterization schemes than the previous CMIP5 experiment. The available scientific results in respect of the CMIP6 show that the CMIP6 improved the ability to simulate climate mean and extreme features of extreme precipitation in China when compared to CMIP5.

In this study, rainfall data from the CMIP6 multi-model ensemble were calculated in order to evaluate the simulation performance of the CMIP6 global climate model for the historical baseline period. Then, the aim was to derive future projections of landslide susceptibility based on CMIP6-based future projections. If the GCM multi-model ensemble can better reproduce the observations in the historical period, it is then considered that the multi-model ensemble is also reasonable for the prediction of future climate change scenarios. Historical rainfall data from 1995–2014 were selected as the baseline for the landslide assessment. The period corresponding to the target temperature rise of 1.5 °C–4.0 °C, as defined in the IPCC Sixth Assessment Report, represents the future period [60] (Table 1).

Table 1. The years corresponding to the different target temperature rise scenarios defined by the IPCC report. The n.c. means that the level was not crossed during the period of 2021–2100.

	SSP1-2.6	SSP2-4.5	SSP5-8.5
1.5 °C	2023–2042	2021–2040	2018–2037
2 °C	n.c.	2043–2062	2032–2051
3 °C	n.c.	n.c.	2055–2074
4 °C	n.c.	n.c.	2075–2094

In respect of the different global climate models, the results of rainfall-induced landslide susceptibility regarding different future warming scenarios were calculated separately and compared with the historical baseline period.

3.4. Evaluation Methods

In this study, the predictive ability of various models was assessed utilizing the area under the receiver operating characteristic curves (AUCs), accuracy, and F1 scores. The area under the receiver operating characteristic curve (AUC) is more closer to one, thereby indicating that the model estimation is more accurate [61,62]. The number of predicted and actual values for landslide points (marked as 1), as well as the non-landslide points (marked as 0) are included in the confusion matrix. Then, the true-positives (i.e., the number of landslides correctly predicted), false-positives (the number of non-landslides predicted as landslides), true-negatives (the number of non-landslides correctly predicted), and false-negatives (the number of landslides predicted as non-landslides) were all computed separately from the confusion matrix, and other performance metrics, such as the ACC and F1 scores, are based on these metrics. Table 2 details the formulas that were utilized in this work for evaluation.

Table 2. List of the predicted performance assessment metrics.

Metric	Formula
ACC(%)	$(TN + TP)/(TN + FN + FP + TP)$
Precision(%)	$TP/(FP + TP)$
Recall(%)	$TP/(FN + TP)$
F1(%)	$(2 \times Recall \times Precision)/(Recall + Precision)$

The method of dividing the 70% training set and 30% validation set has been recognized by most scholars; however, despite this, it lacks spatial information. Due to the spatial autocorrelation phenomena, K-fold cross-validation (CV) with random self-sampling in order to avoid the model overfitting bias were used in this study. The spatial autocorrelation is not directly captured by cross-validation, and the reason for the poor performance of cross-validation is that the dependence structure in the data persists as a dependence structure in the model residuals, which provides ample opportunity for overfitting [63]. Therefore, when modeling with spatially dependent variables is considered, the use of spatial cross-validation (SCV) will provide a better representation of the modeling results [64]. In this regard, we estimated the robustness of diverse machine learning models via using 10-fold cross-validation with 20 repetitions, for a total of 200 CVs and SCVs each. After considering the spatial relationship of each sample, K-fold spatial cross-validation was used in order to separate the dataset into K subsets. Then, the standard error (SE) and quartile deviation were calculated in the same manner as the non-spatial cross-validation to estimate the robustness of the prediction ability. Due to the differences between models [65], the produced landslide susceptibility probability maps use the quantile method in order to ensure that the relative area of each rank is as consistent as possible, thereby allowing for easier contrast of the final results [66].

The R software, which is an open-source data analysis system, was used for all of the quantitative analyses that were conducted in this study. The GAM was implemented with the "mgcv" package, the RF model was conducted with the "ranger" package, and the LightGBM model was conducted with the R packaging "lightgbm". The package "mlr3" was used to perform spatial cross-validation; additionally, please note that the R version used was 4.1.2.

4. Results

4.1. Landslide Dominant Variables in the Hengduan Mountains Region

Regarding the landslide susceptibility analysis, the LCF with the lowest covariance and highest importance should be chosen. The final VIF indices and relative importance ranking of the variables were obtained using different LCFs, and the variables were also introduced into the multiple stepwise regressions, in order to calculate the mutual VIF as shown in Table 3.

Table 3. Results of multicollinearity analysis.

Variable	Relative Importance	VIF	Pr(>|t|)
Slope	0.360	1.488	0.000
Soil type	0.151	1.507	0.000
Curve numbers	0.046	1.821	0.000
CMIP6 simulation of extreme rainfall	0.042	1.659	0.000
Lithology	0.038	1.089	0.001
Soil moisture	0.032	3.577	0.000
Land use	0.015	2.258	0.044
Plan curvature	0.002	1.441	0.058
Profile curvature	0.001	1.450	0.139

The covariance of these variables is less than 5. Additionally, the VIF coefficients range from 1.164 to 3.577, which is considered to be a low covariance. As a result, it is reasonable

to construct a model with these variables. In terms of relative importance, the slope and soil moisture were appraised as two of the most vital influencing determinants in respect of explicating the spatial distribution of landslides in the Hengduan Mountain Region, whereby the relative importance exceeded 15%. This is due to the fact that landslide risk is elevated in areas with high and increasing slope gradients. Soil moisture, a fundamental factor in landslide occurrence, also possesses a strong influence on large-scale landslides. Meanwhile, due to the fact that the relative importance of plan and profile curvature was less than 1%, these two variables were removed from the model training. Then, the remaining seven variables—that is, (a) slope, (b) curve number, (c) frequency over empirical rainfall threshold, (d) soil moisture, (e) lithology, (f) land use, and (g) soil type—were used in subsequent modelling.

4.2. The Predictive Performances of Different Machine Learning Models

We tested the simulation ability of landslide susceptibility by using different machine-learning models during the historical baseline period. The area under the ROC of the model was 0.894 and 0.908, respectively. Moreover, the best models in the validation set were found with the LightGBM and RF (Figure 4). The AUC of GAM model, which possessed the lowest accuracy, was 0.840. All of the models had an AUC greater than 0.8, thereby indicating that different machine-learning models can provide a good estimate of landslide susceptibility in the Hengduan Mountains.
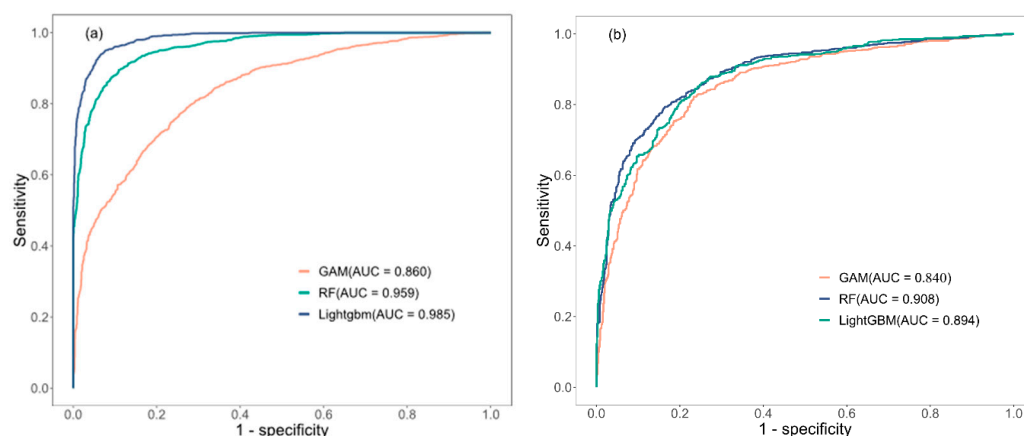

Figure 4. (**a**) The ROC of the training set and (**b**) the ROC of the validation set.

Table 4 shows the ACC and F1 scores for different models in validation. The ACC of the RF, as well as the LightGBM (RF = 0.811, LightGBM = 0.800) and F1-scores (RF = 0.809, LightGBM = 0.800) both exceeded 0.8, thereby indicating that based on the performance in the validation set, the RF and LightGBM models were still the most accurate. This is followed by the GAM (ACC = 0.793, F1 score = 0.783), all of which show that the above models can be utilized for the purposes of landslide susceptibility mapping (LSM).

Table 4. Predictive performance of models on the validation set.

Models	ACC	F1
GAM	0.793	0.783
RF	0.811	0.809
LightGBM	0.800	0.800

Figure 5 indicates that there are similar appearances between the results obtained using non-spatial cross-validation (CV) and those obtained by dividing a training set, thus resulting in these tree models (RF = 0.880, LightGBM = 0.878) remaining the most accurate model. The value in respect of the GAM = 0.840 is the lowest AUC value. The

standard deviation of the AUCs was less than 0.0004 and the quartile deviation was less than 0.04, thereby indicating that the spatial appearance of the landslide susceptibility from the models was in accordance with this. The 20 resampling repetitions, which were conducted by using 10-fold spatial cross-validation (SCV) revealed large fluctuations. The RF showed the greatest prediction estimation accuracy with an AUC of 0.836. Table 5 shows that the AUC decreased by 4.4 percent in contrast to cross-validation. This was obtained with a standard error of 0.009 and an interquartile variance of 0.077, thereby indicating good robustness among all of the models used, as well as the best agreement between the predicted and observed landslides. Meanwhile, the use of spatial cross-validation resulted in greater standard deviations and quartile difference fluctuations, whereby the standard errors of the GAM, RF, and LightGBM were all less than 0.01 (GAM = 0.008, RF = 0.009, and LightGBM = 0.007). Indeed, the RF possessed the smallest change in respect of quartile difference (0.077), followed by the GAM (0.081), and the LightGBM (0.11), all of which possessed changes close to 0.1. In comparison to the non-spatial cross-validation, the degree of uncertainty increased.
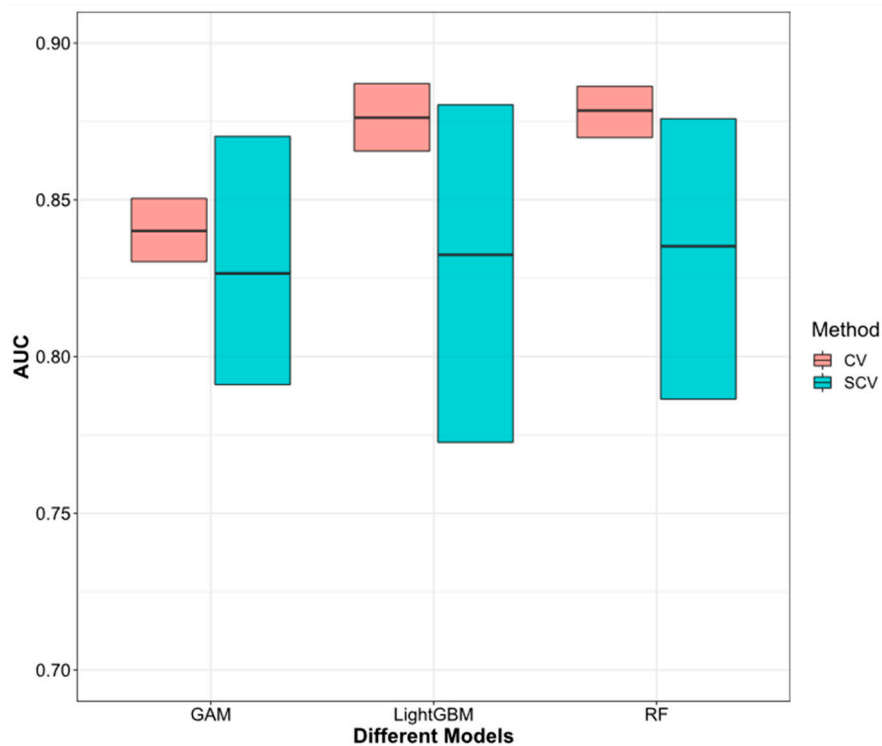

Figure 5. The CV and SCV of different models.

Table 5. Predictive performance of the models on CV and SCV.

Models	CV AUC Mean	CV AUC SE	CV Quartile Deviation	SCV AUC Mean	SCV AUC SE	SCV Quartile Deviation
GAM	0.840	0.00037	0.025	0.826	0.0088	0.081
RF	0.880	0.00025	0.02	0.836	0.0099	0.077
LightGBM	0.878	0.00024	0.019	0.833	0.0074	0.11

4.3. Importance of the Predictors

Determining the relative importance of LCF in various susceptibility models aids in distinguishing the key determinants that affect the occurrence of landslides. Figure 6 shows that the results of various models varied greatly, but soil type was deemed the most important influencing variable. In summary, soil type, soil moisture, slope, and frequency

over extreme rainfall thresholds are the top four variables in regard to importance. The other variables, however, vary considerably in terms of importance among the various models. The results of the assessment regarding the importance of the influencing factors suggest that introducing the projected extreme rainfall into future landslide susceptibility modeling would provide a possible propensity indication in respect of the trend of future landslide susceptibility changes.
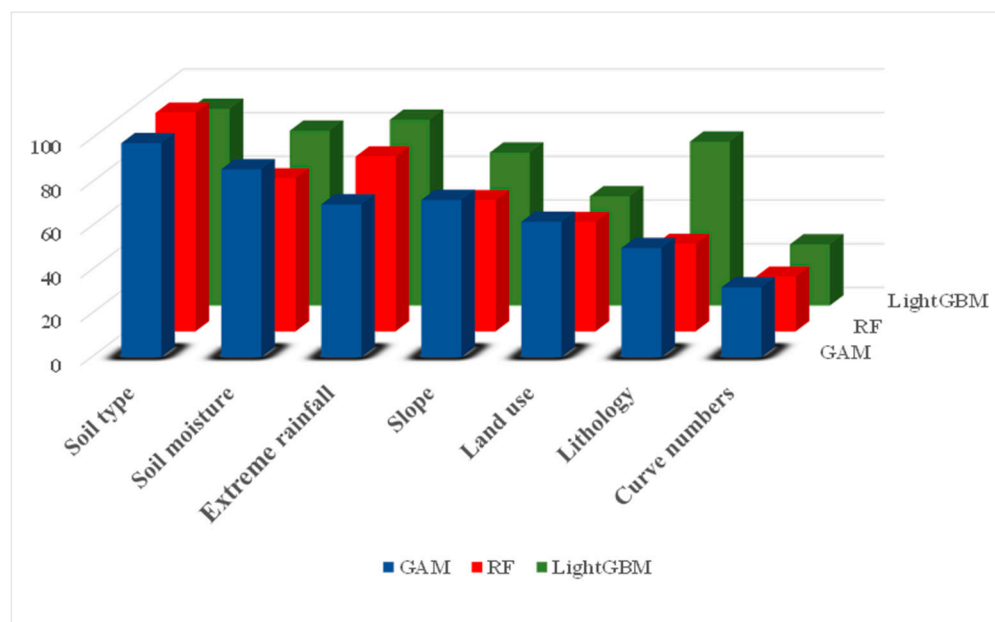

Figure 6. The relative importance of influencing factors by different models.

4.4. Frequency over Empirical Rainfall Threshold Based on the CMIP6

We considered the extreme rainfall scenarios for the CMIP6 for historical period and different future warming scenarios. The observations during historical period were used in order to measure the simulation performance of the CMIP6. In Table 6, the simulated historical rainfall data possessed minimum and maximum values of 1.3 and 12.0, respectively, with a mean value of 6.8 and a standard deviation of 2.0. The extreme values and standard deviations of the related FOERT in respect of the simulated historical period were very close to the historical observation data, while the mean was slightly higher. We also calculated the spatial correlation coefficient of 0.58 for both, which was a moderate correlation. By consulting the relevant literature, the simulated temperature and precipitation values of the CMIP6 were relatively inferior simulated in areas with complex topography and variable climate when compared to flat topography areas. In addition, the simulated FOERT was slightly higher in the study area [67]. However, combined with the results of the model ROC in testing, an AUC value of more than 0.8 was also obtained via the introducing of simulated historical contemporaneous data. This was achieved while the spatial correlation between the two was moderate. In summary, we conclude that the CMIP6 can well simulate the spatial distribution of extreme rainfall in the region.

With increasing projected warming, the minimum value increased from 2.1 to 2.8, the maximum value changed from 11.9 to 13.9, and the mean value increased from 2.3 to 9.0 (with a standard deviation of 1.8 to 2.1). As such, we found that the projected extreme rainfall demonstrated an increasing trend when compared to the historical baseline. Moreover, the maximum value, average value, and standard deviation all increased in conjunction with the increasing warming targets. The rainfall extremes under future scenarios are higher than the historical baseline results, except for the extreme rainfall of 1.5 °C warming, whereby the maximum values were lower than the historical average. The extreme rainfall

indicator was used as an important characterization of future climate in order to produce the LSM under different warming scenarios (Figure 7).

Table 6. Historical FEROT and CMIP6 statistical values regarding simulated rainfall.

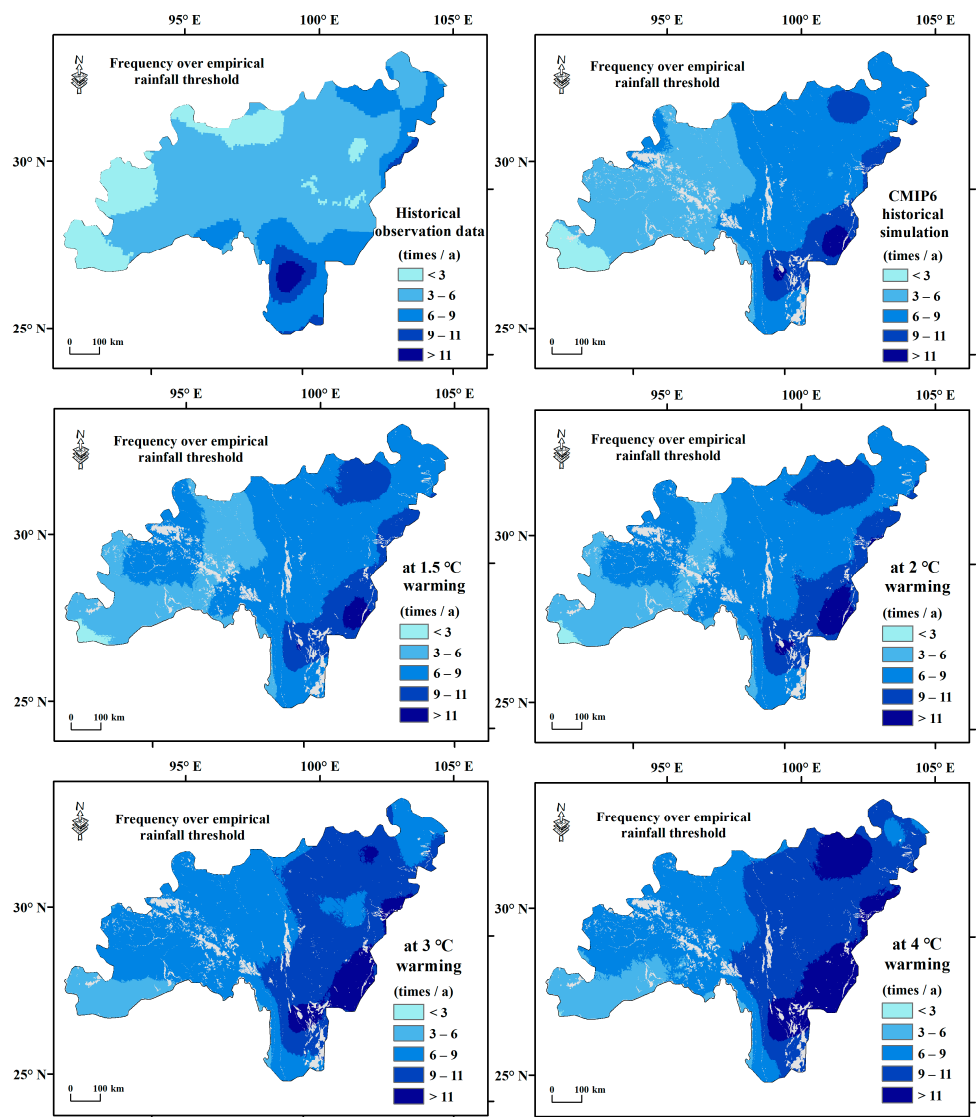| Scenarios (time/a)	Min	Max	Mean	Standard Deviation
Historical	1.5	12.5	4.8	2.1
Historical simulation	1.3	12.0	6.8	2.0
at 1.5 °C	2.1	11.9	2.3	1.8
at 2.0 °C	2.2	12.4	7.6	1.9
at 3.0 °C	3.1	13.1	8.5	1.7
at 4.0 °C	2.8	13.9	9.0	2.1

Figure 7. Frequency over empirical rainfall threshold (FOERT): based on the historical observation, the CMIP6 historical simulation, as well as the future projection under 1.5–4.0 °C warming scenarios.

4.5. Projection of LSM by Considering the Change of Extreme Rainfall

4.5.1. Landslide Susceptibility Map during the Historical Baseline Period

Normalized LCF data were introduced into various machine learning methods in order to obtain LCPs for the whole research area. By using quantile reclassification in the

GIS platform in order to follow up with a better comparison, LSMs were divided into five categories: very low, low, moderate, high, and very high susceptibility levels, as listed in Figure 8a–c. Relative scores for landslide susceptibility in respect of the GAM = 0.71, RF = 0.657, and LightGBM = 0.783 were the obtained thresholds for the high susceptibility regions. Each LSP ranged from 0 to 1; further, the high susceptibility thresholds were all between 0.65 and 0.8. The results obtained by the various models showed a degree of consistent characteristics. The central and southeastern regions, in particular, will be more prone to landslides. Moreover, parts of the northeastern and northwestern regions of the study area also possess the potential to become areas of high landslide susceptibility. Therefore, these LSMs reflect the overall landslide susceptibility and entail significant practical implications in respect of hazard assessments in the Hengduan Mountains.
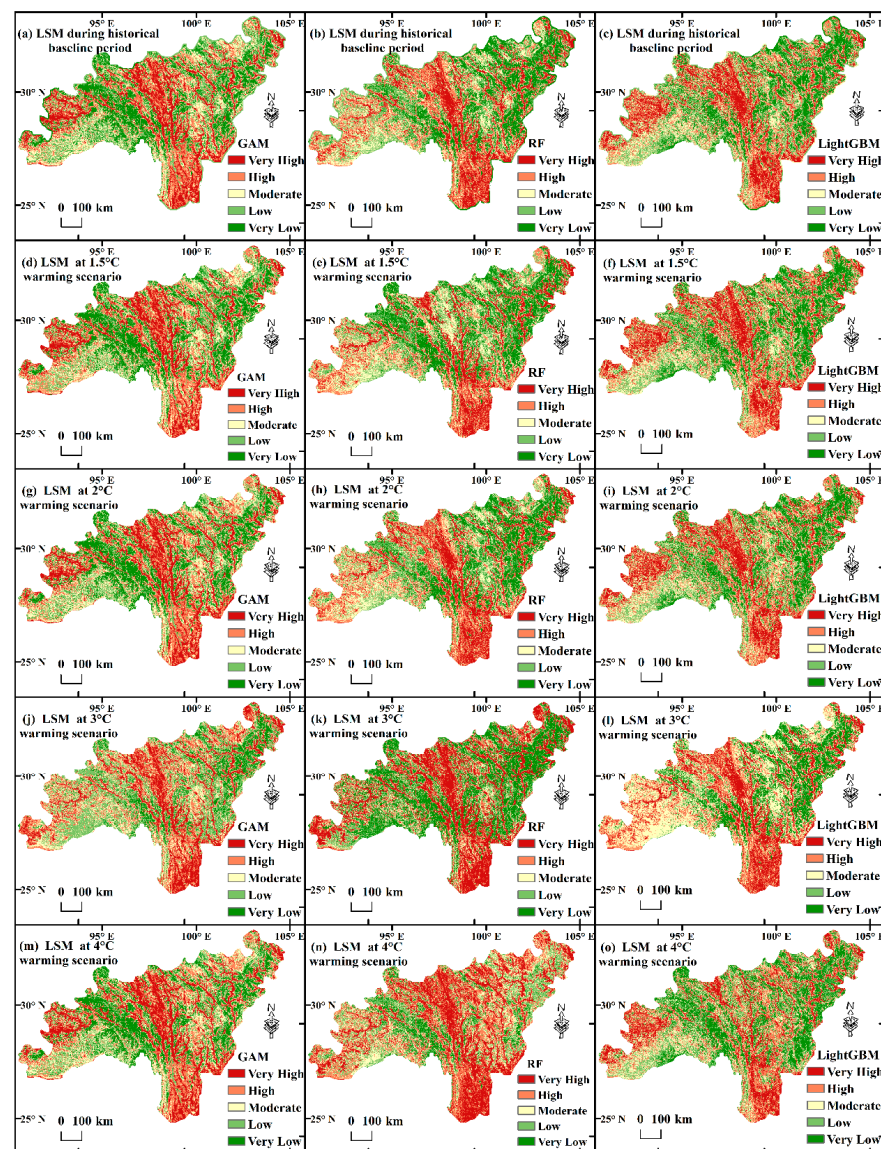

Figure 8. The spatial appearance of landslide susceptibility based on different models for historical and future scenarios: (**a**,**d**,**g**,**j**,**m**) GAM, (**b**,**e**,**h**,**k**,**n**) RF, (**c**,**f**,**i**,**l**,**o**) LightGBM.

4.5.2. Landslide Susceptibility Maps under Different Warming Scenarios

The LSM in respect of the introduction of future extreme rainfall, has been integrated via utilizing different modeling methods. Each map was compared with that of the historical baseline in order to explore the potential future climate change impact on landslide susceptibility in the Hengduan Mountains. The thresholds of the previous quantile quan-

tification were used in a uniform manner in order to facilitate a better comparison with the historical benchmark. As such, the modeling results of the different models were consistent overall. Figure 8 shows the projected LSM that could occur at a global temperature warming of 1.5 °C, 2 °C, 3 °C, and 4 °C, respectively. These results clearly show the trend regarding the influence of rainfall on landslide susceptibility under different warming conditions. Furthermore, it was also observed that there was a significant trend in respect of increasing the area of high susceptibility in the southeast with increasing extreme rainfall. It is expected that the high susceptibility areas will affect an average of 26.1% of the area under a 4 °C warming scenario, which thus means that 26% of the area will be at risk of natural disasters. This finding, therefore, has a key role in aiding future landslide hazard mitigation.

In order to further analyze the specific impact of landslide susceptibility variations due to changes in extreme rainfall, we counted the percentage of the different zones in respect of the LSM produced from different extreme rainfall conditions under different warming scenarios. This was achieved by using the historical LSM threshold as a benchmark. In Figure 9, the LSM high-susceptibility zones that were derived from the GAM and RF models increased with an increase of warming. Regarding the LSM that was depicted by the GAM, the percentage of low susceptibility zones decreased to 19%, and the percentage of high susceptibility zones increased to 22% as the temperature increased. The LSM results extrapolated from the RF show that the proportion of low susceptibility zones decreased to 12.8%, while the proportion of high susceptibility zones reached 26%. Although there is no particularly clear trend in the LightGBM model, the high susceptibility area increased by 2.1% on average in the 4 °C scenarios, with an actual increase in the impact area of around 11,578 km^2. In summary, the landslide susceptibility in the Hengduan Mountain Region becomes more active with an increase in extreme rainfall. These results are reasonably consistent with the findings obtained from existing studies. The prevention of natural hazards will be more challenging in the future.
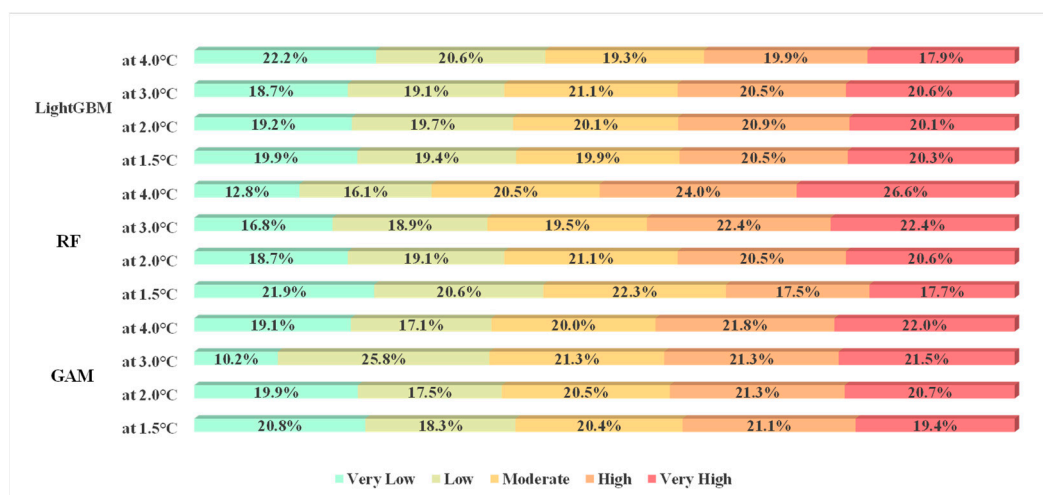

Figure 9. Percentage of different landslide susceptibility classes under different warming scenarios.

5. Discussion

In this study, the impact of climate change on landslides in the Hengduan Mountain Region was quantitatively assessed. This was achieved by considering the variation in extreme rainfall under different global warming scenarios and feeding this data to various machine learning-based landslide susceptibility models. The results show that the simulation of the CMIP6 overall has a good fit in respect of EFORT for the historical period. Furthermore, the EFORT also indicates an increasing trend in the future with an increase of warming, while the potential impact area of the high susceptibility will also become larger. When the climate temperature increases by 4 °C, the high landslide susceptibility

area increases significantly; as such, corresponding climate change measures were required in the central and southeastern parts of the study area in order to mitigate the potential risk of landslide occurrence.

The model-derived variables such as soil type, soil moisture, slope, and extreme rainfall became the most dominant variables in the study area. The results are mostly consistent with the results of Zhao et al., (2022) [18], but we additionally focused on the potential impact of climate change, which is closer to the real LSM that is designed considering future perspectives in this work. The results of several studies have shown that rainfall is an important factor for changing regional slope stability [68]. In this study, it was also revealed that the frequency of extreme rainfall thresholds (FOERT) tends to increase with warming targets, thereby ranging from 2.3/a (at a 1.5 °C warming) to 9.0/a (at a 4.0 °C warming) on average. Therefore, it is particularly important to consider landslide susceptibility predictions within the context of future rainfall scenarios. Through conducting this research, it was determined to be exposed that such elevated extreme precipitation events contribute to an increase in the projected future zones of high landslide susceptibility, while using different machine learning models, when compared to the historical baseline period ranging from -1.2% (at a 1.5 °C warmings) to 4.0% (at a 4.0 °C warming). This finding is in agreement with the results of existing studies [69]. Indeed, more studies show that projection results which take climate change into account will be more conducive in respect of more accurate diagnoses of natural disasters. However, this also comes with the understanding that future occurrences of extreme weather are likely to be more frequent. Therefore, considering landslide susceptibility estimates within the context of global warming scenarios will be more beneficial for the purposes of natural disaster prevention.

Although the results of this study have fairly high accuracy in model evaluation, these methods do not account for all factors that contribute to landslide occurrence, thereby rendering the process more complex. While the soil type discovered in the study aids in data prediction, the intrinsic nature of soil properties and the occurrence of landslides must also be investigated [70]. The complexity of landslide occurrence and the geographical variety of regional variables may impair the accuracy of landslide estimations [71]. Certain scholars have also considered the dynamic changes in land use, which have proved to be more beneficial for the purposes of dynamic landslide susceptibility assessment [72]. In any case, considering the impact of future climate change-induced rainfall values will provide new ideas for the assessment of natural hazards.

In this study, it is clearly shown that the highly susceptible areas in the Hengduan Mountains will be more affected by increased rainfall in the future. Therefore, it is helpful for the purposes of landslide susceptibility prediction when dynamic rainfall factors are considered [73,74]. The effect of cumulative rainfall thresholds on landslides in a specific period was not considered in this study; on this note, it would be more beneficial to introduce specific rainfall events in a specific period and add a temporal dimension to the LSM [75]. In any case, in this work, the potential impact of EFORT in reflecting climate change on landslide susceptibility in the Hengduan Mountains under the different scenarios of 1.5 °C, 2 °C, 3 °C, and 4 °C warmings, which will be a key step for future studies in terms of considering the impact of climate change on natural hazards, is integrated.

Furthermore, a future extreme rainfall-induced landslide that will increase over the study area is indicated in this work. As climate change-induced global warming intensifies, human causalities from landslides are expected to increase in the future. Therefore, through our study we urge strong policy interventions in order to reduce such socioeconomic damage and deaths from these potential future landslides. Indeed, two main aspects should be considered, such as climate change mitigation through CO_2 emission cuts and adaptation, as well as prevention of landslide events. The IPCC (2018) documented the fact that, in order to constrain the global warming level at 1.5 °C, global net CO_2 emission is expected to decline around 45% by 2030, and thus, for net-zero levels to be attained by 2045–2055. In order to lock warming below 2.0 °C, human-induced CO_2 emissions are predicted

to reduce by 25% by 2030; in addition, it has been forecasted that a net-zero level will be achieved by the 2065–2080 period. Therefore, our findings highlight the accomplishment of the global emissions mitigation goal that was agreed under the Paris Agreement. Further, in order to avoid landslide impacts over the area, certain precautionary measures could be taken, such as restriction or even removing of populations from the landslide-prone area, controlling certain types of land use where slope stability is fragile, and adopting an early warning system based on ground condition monitoring, such as: slope dislocation; soil and rock types; and groundwater levels. Indeed, several measures can help to mitigate and prevent landslides over the study area, such as modifying slope geometry, adopting reinforced slope material, installing piles, retaining walls, diverting debris pathways, and re-routing surface and groundwater passways.

6. Conclusions

In this study, the potential impact of climate change on landslide susceptibility in the Hengduan Mountains of China, while using the latest multi-model climate ensemble of CMIP6, was quantitatively estimated. We utilized the GAM, RF, and LightGBM in order to quantitatively assess the predictive power of the CMIP6 for landslide susceptibility. The AUC of all models exceeded 80%, and the correlation coefficient with historical observations was 0.58, thereby indicating that the CMIP6 possesses a good ability to fit the rainfall values in historical periods. Soil type, soil moisture, slope, and the frequency over extreme rainfall thresholds are the top four variables in terms of importance. The results of the analyses all provide evidence that the considering future rainfall scenarios to be closer to the real situation and that the probability of natural hazards will increase significantly as the degree of global warming continues to increase. When climate warming reaches 4 °C above pre-industrial levels, the maximum value of the EFORT is close to 14, and the projected LSM indicates that the area of the high susceptibility zone increases substantially. The central and southeastern parts of the Hengduan Mountains are the regions with the highest susceptibility to natural hazards. Therefore, these areas must be given priority when implementing conservation measures, such as those taken in response to climate change. We need to take appropriate measures in order to adapt to the effects of climate change, as well as to better mitigate the risk of landslide in order to reduce the potential risk of global warming.

Author Contributions: Q.L. Conceptualization, Funding acquisition, Supervision; H.Y. and J.Z. Writing—original draft; H.Y., J.Z., S.K.M., B.W., L.Z., L.W. and Q.L. Writing—review & editing. All authors have read and agreed to the published version of the manuscript.

Institutional Review Board Statement: Not applicable.

Informed Consent Statement: Not applicable.

Data Availability Statement: Not applicable.

Conflicts of Interest: The authors declare that the research was conducted in the absence of any commercial or financial relationships that could be construed as a potential conflict of interest.

References

1. Camera, C.A.; Bajni, G.; Corno, I.; Raffa, M.; Stevenazzi, S.; Apuani, T. Introducing intense rainfall and snowmelt variables to implement a process-related non-stationary shallow landslide susceptibility analysis. *Sci. Total. Environ.* **2021**, *786*, 147360. [CrossRef]

2. Masson-Delmotte, V.; Zhai, P.; Pörtner, H.O.; Roberts, D.; Skea, J.; Shukla, P.R.; Pirani, A.; Moufouma-Okia, W.; Péan, C.; Pidcock, R.; et al. Global warming of 1.5 °C. In *An IPCC Special Report on the Impacts of Global Warming of Globle Warming*; IPCC: Geneva, Switzerland, 2018.

3. Gariano, S.; Rianna, G.; Petrucci, O.; Guzzetti, F. Assessing future changes in the occurrence of rainfall-induced landslides at a regional scale. *Sci. Total. Environ.* **2017**, *596–597*, 417–426. [CrossRef]

4. Kirschbaum, D.; Kapnick, S.B.; Stanley, T.; Pascale, S. Changes in Extreme Precipitation and Landslides Over High Mountain Asia. *Geophys. Res. Lett.* **2020**, *47*, e2019GL085347. [CrossRef]

5. Maraun, D.; Knevels, R.; Mishra, A.N.; Truhetz, H.; Bevacqua, E.; Proske, H.; Zappa, G.; Brenning, A.; Petschko, H.; Schaffer, A.; et al. A severe landslide event in the Alpine foreland under possible future climate and land-use changes. *Commun. Earth Environ.* **2022**, *3*, 87. [CrossRef]

6. Crozier, M.J. Deciphering the effect of climate change on landslide activity: A review. *Geomorphology* **2010**, *124*, 260–267. [CrossRef]

7. Gariano, S.L.; Guzzetti, F. Landslides in a changing climate. *Earth Sci. Rev.* **2016**, *162*, 227–252. [CrossRef]

8. Gariano, S.L.; Guzzetti, F. Mass-movements and climate change. In *Treatise on Geomorphology*, 2nd ed.; Reference Module in Earth Systems and Environmental Sciences; Elsevier: Amsterdam, The Netherlands, 2022. [CrossRef]

9. Marengo, J.A.; Alves, L.M.; Ambrizzi, T.; Young, A.; Barreto, N.J.C.; Ramos, A.M. Trends in extreme rainfall and hydrogeometeorological disasters in the Metropolitan Area of São Paulo: A review. *Ann. N. Y. Acad. Sci.* **2020**, *1472*, 5–20. [CrossRef]

10. Chowdhuri, I.; Pal, S.C.; Chakrabortty, R.; Malik, S.; Das, B.; Roy, P.; Sen, K. Spatial prediction of landslide susceptibility using projected storm rainfall and land use in Himalayan region. *Bull. Eng. Geol. Environ.* **2021**, *80*, 5237–5258. [CrossRef]

11. Pham, Q.B.; Pal, S.C.; Chakrabortty, R.; Saha, A.; Janizadeh, S.; Ahmadi, K.; Khedher, K.M.; Anh, D.T.; Tiefenbacher, J.P.; Bannari, A. Predicting landslide susceptibility based on decision tree machine learning models under climate and land use changes. *Geocarto Int.* **2021**. [CrossRef]

12. Lin, Q.; Wang, Y.; Glade, T.; Zhang, J.; Zhang, Y. Assessing the spatiotemporal impact of climate change on event rainfall characteristics influencing landslide occurrences based on multiple GCM projections in China. *Clim. Chang.* **2020**, *162*, 761–779. [CrossRef]

13. Ciabatta, L.; Camici, S.; Brocca, L.; Ponziani, F.; Stelluti, M.; Berni, N.; Moramarco, T. Assessing the impact of climate-change scenarios on landslide occurrence in Umbria Region, Italy. *J. Hydrol.* **2016**, *541*, 285–295. [CrossRef]

14. Peres, D.J.; Cancelliere, A. Modeling impacts of climate change on return period of landslide triggering. *J. Hydrol.* **2018**, *567*, 420–434. [CrossRef]

15. Li, M.; Tian, C.-S.; Wang, Y.-K.; Liu, Q.; Lu, Y.-F.; Shan, W. Impacts of future climate change (2030-2059) on debris flow hazard: A case study in the Upper Minjiang River basin, China. *J. Mt. Sci.* **2018**, *15*, 1836–1850. [CrossRef]

16. He, S.; Wang, J.; Wang, H. Projection of Landslides in China during the 21st Century under the RCP8.5 Scenario. *J. Meteorol. Res.* **2019**, *33*, 138–148. [CrossRef]

17. Lin, Q.; Steger, S.; Pittore, M.; Zhang, J.; Wang, L.; Jiang, T.; Wang, Y. Evaluation of potential changes in landslide susceptibility and landslide occurrence frequency in China under climate change. *Sci. Total. Environ.* **2022**, *850*, 158049. [CrossRef]

18. Zhao, J.; Zhang, Q.; Wang, D.; Wu, W.; Yuan, R. Machine Learning-Based Evaluation of Susceptibility to Geological Hazards in the Hengduan Mountains Region, China. *Int. J. Disaster Risk Sci.* **2022**, *13*, 305–316. [CrossRef]

19. Liu, C.; Li, W.; Wu, H.; Lu, P.; Sang, K.; Sun, W.; Chen, W.; Hong, Y.; Li, R. Susceptibility evaluation and mapping of China's landslides based on multi-source data. *Nat. Hazards* **2013**, *69*, 1477–1495. [CrossRef]

20. Li, Z.; He, Y.; Wang, C.; Wang, X.; Xin, H.; Zhang, W.; Cao, W. Spatial and temporal trends of temperature and precipitation during 1960–2008 at the Hengduan Mountains, China. *Quat. Int.* **2011**, *236*, 127–142. [CrossRef]

21. Zhu, Y.; Yang, S. Evaluation of CMIP6 for historical temperature and precipitation over the Tibetan Plateau and its comparison with CMIP5. *Adv. Clim. Chang. Res.* **2020**, *11*, 239–251. [CrossRef]

22. Almazroui, M.; Saeed, S.; Saeed, F.; Islam, M.N.; Ismail, M. Projections of Precipitation and Temperature over the South Asian Countries in CMIP6. *Earth Syst. Environ.* **2020**, *4*, 297–320. [CrossRef]

23. Xu, H.; Chen, H.; Wang, H. Future changes in precipitation extremes across China based on CMIP6 models. *Int. J. Clim.* **2022**, *42*, 635–651. [CrossRef]

24. Zhu, H.; Jiang, Z.; Li, J.; Li, W.; Sun, C.; Li, L. Does CMIP6 inspire more confidence in simulating climate extremes over China? *Adv. Atmos. Sci.* **2020**, *37*, 1119–1132. [CrossRef]

25. Wei, L.; Hu, K.; Liu, S. Spatial distribution of debris flow-prone catchments in Hengduan mountainous area in southwestern China. *Arab. J. Geosci.* **2021**, *14*, 2650. [CrossRef]

26. Wu, W.; Zhang, Q.; Singh, V.P.; Wang, G.; Zhao, J.; Shen, Z.; Sun, S. A Data-Driven Model on Google Earth Engine for Landslide Susceptibility Assessment in the Hengduan Mountains, the Qinghai–Tibetan Plateau. *Remote Sens.* **2022**, *14*, 4662. [CrossRef]

27. Guzzetti, F.; Carrara, A.; Cardinali, M.; Reichenbach, P. Landslide hazard evaluation: A review of current techniques and their application in a multi-scale study, Central Italy. *Geomorphology* **1999**, *31*, 181–216. [CrossRef]

28. Lin, Q.; Wang, Y. Spatial and temporal analysis of a fatal landslide inventory in China from 1950 to 2016. *Landslides* **2018**, *15*, 2357–2372. [CrossRef]

29. Lin, Q.; Lima, P.; Steger, S.; Glade, T.; Jiang, T.; Zhang, J.; Liu, T.; Wang, Y. National-scale data-driven rainfall induced landslide susceptibility mapping for China by accounting for incomplete landslide data. *Geosci. Front.* **2021**, *12*, 101248. [CrossRef]

30. Reichenbach, P.; Rossi, M.; Malamud, B.D.; Mihir, M.; Guzzetti, F. A review of statistically-based landslide susceptibility models. *Earth Sci. Rev.* **2018**, *180*, 60–91. [CrossRef]
31. Chen, W.; Panahi, M.; Tsangaratos, P.; Shahabi, H.; Ilia, I.; Panahi, S.; Li, S.; Jaafari, A.; Bin Ahmad, B. Applying population-based evolutionary algorithms and a neuro-fuzzy system for modeling landslide susceptibility. *Catena* **2019**, *172*, 212–231. [CrossRef]
32. Roccati, A.; Paliaga, G.; Luino, F.; Faccini, F.; Turconi, L. GIS-Based Landslide Susceptibility Mapping for Land Use Planning and Risk Assessment. *Land* **2021**, *10*, 162. [CrossRef]
33. Ponziani, F.; Pandolfo, C.; Stelluti, M.; Berni, N.; Brocca, L.; Moramarco, T. Assessment of rainfall thresholds and soil moisture modeling for operational hydrogeological risk prevention in the Umbria region (central Italy). *Landslides* **2012**, *9*, 229–237. [CrossRef]
34. Nhu, V.-H.; Shirzadi, A.; Shahabi, H.; Chen, W.; Clague, J.J.; Geertsema, M.; Jaafari, A.; Avand, M.; Miraki, S.; Asl, D.T.; et al. Shallow Landslide Susceptibility Mapping by Random Forest Base Classifier and Its Ensembles in a Semi-Arid Region of Iran. *Forests* **2020**, *11*, 421. [CrossRef]
35. Costanzo, D.; Rotigliano, E.; Irigaray, C.; Jiménez-Perálvarez, J.D.; Chacón, J. Factors selection in landslide susceptibility modelling on large scale following the gis matrix method: Application to the river Beiro basin (Spain). *Nat. Hazards Earth Syst. Sci.* **2012**, *12*, 327–340. [CrossRef]
36. Sajadi, P.; Singh, A.; Mukherjee, S.; Luo, P.; Chapi, K.; Salari, M. Multivariate statistical analysis of relationship between tectonic activity and drainage behavior in Qorveh-Dehgolan basin Kurdistan, Iran. *Geocarto Int.* **2021**, *36*, 540–562. [CrossRef]
37. Catani, F.; Lagomarsino, D.; Segoni, S.; Tofani, V. Landslide susceptibility estimation by random forests technique: Sensitivity and scaling issues. *Nat. Hazards Earth Syst. Sci.* **2013**, *13*, 2815–2831. [CrossRef]
38. Choi, J.; Oh, H.-J.; Lee, H.-J.; Lee, C.; Lee, S. Combining landslide susceptibility maps obtained from frequency ratio, logistic regression, and artificial neural network models using ASTER images and GIS. *Eng. Geol.* **2012**, *124*, 12–23. [CrossRef]
39. Zhao, G.; Pang, B.; Xu, Z.; Yue, J.; Tu, T. Mapping flood susceptibility in mountainous areas on a national scale in China. *Sci. Total. Environ.* **2018**, *615*, 1133–1142. [CrossRef]
40. Wang, B.; Lin, Q.; Jiang, T.; Yin, H.; Zhou, J.; Sun, J.; Wang, D.; Dai, R. Evaluation of linear, nonlinear and ensemble machine learning models for landslide susceptibility assessment in Southwest China. *Geocarto Int.* **2022**, 2152493. [CrossRef]
41. Trabucco, A.; Zomer, R.J. Global High-Resolution Soil-Water Balance. Figshare, Dataset. 2019. Available online: https://figshare.com/articles/dataset/Global_High-Resolution_Soil-Water_Balance/7707605/3 (accessed on 11 December 2022).
42. Wu, J.; Gao, X.J. A gridded daily observation dataset over China region and comparison with the other datasets. *Chin. J. Geophys.* **2013**, *56*, 1102–1111. [CrossRef]
43. Wang, N.; Lombardo, L.; Gariano, S.L.; Cheng, W.; Liu, C.; Xiong, J.; Wang, R. Using satellite rainfall products to assess the triggering conditions for hydro-morphological processes in different geomorphological settings in China. *Int. J. Appl. Earth Obs. Geoinformation* **2021**, *102*, 102350. [CrossRef]
44. Linke, S.; Lehner, B.; Dallaire, C.O.; Ariwi, J.; Grill, G.; Anand, M.; Beames, P.; Burchard-Levine, V.; Maxwell, S.; Moidu, H.; et al. Global hydro-environmental sub-basin and river reach characteristics at high spatial resolution. *Sci. Data* **2019**, *6*, 283. [CrossRef]
45. Heckmann, T.; Gegg, K.; Gegg, A.; Becht, M. Sample size matters: Investigating the effect of sample size on a logistic regression susceptibility model for debris flows. *Nat. Hazards Earth Syst. Sci.* **2014**, *14*, 259–278. [CrossRef]
46. Romer, C.; Ferentinou, M. Shallow landslide susceptibility assessment in a semiarid environment—A Quaternary catchment of KwaZulu-Natal, South Africa. *Eng. Geol.* **2016**, *201*, 29–44. [CrossRef]
47. Kornejady, A.; Ownegh, M.; Bahremand, A. Landslide susceptibility assessment using maximum entropy model with two different data sampling methods. *Catena* **2017**, *152*, 144–162. [CrossRef]
48. Chen, W.; Peng, J.; Hong, H.; Shahabi, H.; Pradhan, B.; Liu, J.; Zhu, A.-X.; Pei, X.; Duan, Z. Landslide susceptibility modelling using GIS-based machine learning techniques for Chongren County, Jiangxi Province, China. *Sci. Total. Environ.* **2018**, *626*, 1121–1135. [CrossRef]
49. Sajadi, P.; Sang, Y.-F.; Gholamnia, M.; Bonafoni, S.; Mukherjee, S. Evaluation of the landslide susceptibility and its spatial difference in the whole Qinghai-Tibetan Plateau region by five learning algorithms. *Geosci. Lett.* **2022**, *9*, 9. [CrossRef]
50. Ikram, N.; Basharat, M.; Ali, A.; Usmani, N.A.; Gardezi, S.A.H.; Hussain, M.L.; Riaz, M.T. Comparison of landslide susceptibility models and their robustness analysis: A case study from the NW Himalayas, Pakistan. *Geocarto Int.* **2021**. [CrossRef]
51. O'Brien, R.M. A Caution Regarding Rules of Thumb for Variance Inflation Factors. *Qual. Quant.* **2007**, *41*, 673–690. [CrossRef]
52. TonidandelJames, S.; LeBreton, J. Relative Importance Analysis: A Useful Supplement to Regression Analysis. *J. Bus. Psychol.* **2011**, *26*, 1–9. [CrossRef]
53. Groemping, U. Relative Importance for Linear Regression in R: The Packagerelaimpo. *J. Stat. Softw.* **2006**, *17*, 1–27. [CrossRef]
54. Wang, C.; Lin, Q.; Wang, L.; Jiang, T.; Su, B.; Wang, Y.; Mondal, S.K.; Huang, J.; Wang, Y. The influences of the spatial extent selection for non-landslide samples on statistical-based landslide susceptibility modelling: A case study of Anhui Province in China. *Nat. Hazards* **2022**, *112*, 1967–1988. [CrossRef]
55. Brenning, A.; Long, S.; Fieguth, P. Detecting rock glacier flow structures using Gabor filters and IKONOS imagery. *Remote Sens. Environ.* **2012**, *125*, 227–237. [CrossRef]
56. Goetz, J.N.; Brenning, A.; Petschko, H.; Leopold, P. Evaluating machine learning and statistical prediction techniques for landslide susceptibility modeling. *Comput. Geosci.* **2015**, *81*, 1–11. [CrossRef]

57. Sahin, E.K. Comparative analysis of gradient boosting algorithms for landslide susceptibility mapping. *Geocarto Int.* **2020**, *37*, 2441–2465. [CrossRef]
58. Steger, S.; Mair, V.; Kofler, C.; Pittore, M.; Zebisch, M.; Schneiderbauer, S. Correlation does not imply geomorphic causation in data-driven landslide susceptibility modelling–Benefits of exploring landslide data collection effects. *Sci. Total. Environ.* **2021**, *776*, 145935. [CrossRef]
59. Ke, G.; Meng, Q.; Finley, T.; Wang, T.; Chen, W.; Ma, W.; Ye, Q.; Liu, T.-Y. Lightgbm: A highly efficient gradient boosting decision tree. *Adv. Neural Inf. Process. Syst.* **2017**, 30.
60. IPCC-Intergovernmental Panel on Climate Change. *Climate Change 2021: The Physical Science Basis. Contribution of Working Group I to the Sixth Assessment Report of the Intergovernmental Panel on Climate Change*; Masson-Delmotte, V., Zhai, P., Pirani, A., Connors, S.L., Péan, C., Berger, S., Caud, N., Chen, Y., Goldfarb, L., Gomis, M.I., et al., Eds.; Cambridge University Press: Cambridge, UK; New York, NY, USA, 2021.
61. Brenning, A.; Trombotto, D. Logistic regression modeling of rock glacier and glacier distribution: Topographic and climatic controls in the semi-arid Andes. *Geomorphology* **2006**, *81*, 141–154. [CrossRef]
62. Guzzetti, F.; Reichenbach, P.; Ardizzone, F.; Cardinali, M.; Galli, M. Estimating the quality of landslide susceptibility models. *Geomorphology* **2006**, *81*, 166–184. [CrossRef]
63. Roberts, D.R.; Bahn, V.; Ciuti, S.; Boyce, M.; Elith, J.; Guillera-Arroita, G.; Hauenstein, S.; Lahoz-Monfort, J.J.; Schroder, B.; Thuiller, W.; et al. Cross-validation strategies for data with temporal, spatial, hierarchical, or phylogenetic structure. *Ecography* **2017**, *40*, 913–929. [CrossRef]
64. Chen, W.; Xie, X.; Wang, J.; Pradhan, B.; Hong, H.; Bui, D.T.; Duan, Z.; Ma, J. A comparative study of logistic model tree, random forest, and classification and regression tree models for spatial prediction of landslide susceptibility. *Catena* **2017**, *151*, 147–160. [CrossRef]
65. Rahmati, O.; Tahmasebipour, N.; Haghizadeh, A.; Pourghasemi, H.R.; Feizizadeh, B. Evaluation of different machine learning models for predicting and mapping the susceptibility of gully erosion. *Geomorphology* **2017**, *298*, 118–137. [CrossRef]
66. Chung, C.-J.F.; Fabbri, A.G. Validation of Spatial Prediction Models for Landslide Hazard Mapping. *Nat. Hazards* **2003**, *30*, 451–472. [CrossRef]
67. Yang, X.; Zhou, B.; Xu, Y.; Han, Z. CMIP6 Evaluation and Projection of Temperature and Precipitation over China. *Adv. Atmos. Sci.* **2021**, *38*, 817–830. [CrossRef]
68. Roy, P.; Pal, S.C.; Chakrabortty, R.; Chowdhuri, I.; Malik, S.; Das, B. Threats of climate and land use change on future flood susceptibility. *J. Clean. Prod.* **2020**, *272*, 122757. [CrossRef]
69. Cao, J.; Zhang, Z.; Wang, C.; Liu, J.; Zhang, L. Susceptibility assessment of landslides triggered by earthquakes in the Western Sichuan Plateau. *Catena* **2019**, *175*, 63–76. [CrossRef]
70. Wang, Y.; Lin, Q.; Shi, P. Spatial pattern and influencing factors of landslide casualty events. *J. Geogr. Sci.* **2018**, *28*, 259–274. [CrossRef]
71. Che, V.B.; Fontijn, K.; Ernst, G.G.; Kervyn, M.; Elburg, M.; Van Ranst, E.; Suh, C.E. Evaluating the degree of weathering in landslide-prone soils in the humid tropics: The case of Limbe, SW Cameroon. *Geoderma* **2012**, *170*, 378–389. [CrossRef]
72. Bordoni, M.; Galanti, Y.; Bartelletti, C.; Persichillo, M.G.; Barsanti, M.; Giannecchini, R.; Avanzi, G.D.; Cevasco, A.; Brandolini, P.; Galve, J.P.; et al. The influence of the inventory on the determination of the rainfall-induced shallow landslides susceptibility using generalized additive models. *Catena* **2020**, *193*, 104630. [CrossRef]
73. Khatun, M.; Hossain, A.T.M.S.; Sayem, H.M.; Moniruzzaman, M.; Ahmed, Z.; Rahaman, K.R. Landslide Susceptibility Mapping Using Weighted-Overlay Approach in Rangamati, Bangladesh. *Earth Syst. Environ.* **2022**. [CrossRef]
74. Dikshit, A.; Satyam, N.; Pradhan, B. Estimation of Rainfall-Induced Landslides Using the TRIGRS Model. *Earth Syst. Environ.* **2019**, *3*, 575–584. [CrossRef]
75. Segoni, S.; Piciullo, L.; Gariano, S.L. A review of the recent literature on rainfall thresholds for landslide occurrence. *Landslides* **2018**, *15*, 1483–1501. [CrossRef]